Biosaintifika 18 (2) (2026): 296-306 p-ISSN 2085-191X | e-ISSN 2338-7610
Journal of Biology & Biology Education https://journal.unnes.ac.id/nju/index.php/biosaintifika

Characterization and Antibacterial Activity of Biosynthesized Zinc Oxide–Silver (ZnO–Ag) Nanocomposites Using *Manihot esculenta* Leaf Extract

Wardah Radhwa Hafizhah[1], Ari Susilowati[1*], Artini Pangastuti[1], Muhammad Ali[2]

[1]Department of Biology, Faculty of Mathematics and Natural Sciences, Sebelas Maret University, Jl. Ir. Sutami, Surakarta, Central Java 57126, Indonesia
[2]Department of Life Sciences, Abasyn University, Islamabad Campus, Park Road, Islamabad 44000, Pakistan

[*]Corresponding author: arisusilowati@staff.uns.ac.id

Submitted: 2026-03-29. Revised: 2026-06-03. Accepted: 2026-08-04.

Abstract. *Pseudomonas aeruginosa*, an important opportunistic pathogen responsible for nosocomial infections, poses a threat in clinical care. Metal-metal oxide nanocomposites have been developed as antibacterial agents due to their synergistic effects. In this study, zinc oxide-silver nanocomposites (ZnO–AgNCs) were synthesized using *Manihot esculenta* leaf extract as a bioreductant, with extract concentrations of 5%, 10%, and 15% (v/v) and $AgNO_3$ concentrations of 6 and 8 mM. The samples were characterized using UV-Vis spectrophotometry, PSA, SEM-EDX, and their antibacterial activity was tested using the disk diffusion method. The best formulation was obtained for ZnO–AgNCs with 5% extract + 8 mM $AgNO_3$, which exhibited an SPR peak at 331 nm and an average particle size of 48.04 nm. SEM-EDX revealed an irregular and agglomerated morphology and confirmed the presence of Zn, O, and Ag. The nanocomposite showed strong antibacterial activity against *P. aeruginosa* with an inhibition zone of 15.83±0.64 mm. These findings highlight its potential for further development in infection control, particularly in medical applications. This study supports the Sustainable Development Goal (SDGs) on Good Health and Well-being (No. 3) through the development of antibacterial materials.

Keywords: antibacterials; biosynthesis; cassava leaf extract; *Pseudomonas aeruginosa;* zinc oxide silver nanocomposite

How to Cite: Hafizhah, W. R., Susilowati, A., Pangastuti, A., & Ali, M. (2026). Characterization and Antibacterial Activity of Biosynthesized Zinc Oxide–Silver (ZnO–Ag) Nanocomposites Using Manihot esculenta Leaf Extract. *Biosaintifika: Journal of Biology & Biology Education, 18(2)*, 296-306.

DOI: http://dx.doi.org/10.15294/biosaintifika.v18i2.40659

INTRODUCTION

Pseudomonas aeruginosa, a Gram-negative bacterium, is an important opportunistic pathogen. Infections caused by this bacterium are frequently encountered in clinical settings, particularly as part of nosocomial infections. This bacterium can infect patients, especially those who are immunocompromised (Thi et al., 2020; Qin et al., 2022). It is responsible for several infections, which include urinary tract infection, septicaemia, osteomyelitis, and endocarditis, making it a serious threat in clinical settings (Palanisamy et al., 2014). Moreover, its persistence on the surfaces of medical devices contributes to healthcare-associated infections and complicates treatment strategies (Reynolds & Kollef, 2021; Moser et al., 2021). Therefore, the development of nanoparticle-based antibacterial agents represents a promising strategy to inhibit bacterial growth and prevent these infections.

Nanoparticles (NPs) are defined as nanoscale (1-100 nm) particles with distinctive physicochemical properties (Chausali et al., 2022). NPs possess a high surface area-to-volume ratio (Khan et al., 2019) and exhibit antibacterial activity by disrupting bacterial membrane integrity (Sali et al., 2021). Nanotechnology has been used in many different applications, such as in the medical field. Numerous studies have reported the use of zinc oxide nanoparticles (ZnONPs) as an antibacterial agent. This includes the report by Sirelkhatim et al. (2015), who documented the antibacterial effect of ZnONPs in *P.aeruginosa*, *Escherichia coli*, *Staphylococcus aureus*, and *Enterococcus faecalis*. Their antibacterial effects arise from the generation of reactive oxygen species (ROS) under light exposure and the release of Zn^{2+} ions under light-independent conditions. The antibacterial performance of NPs can be further enhanced by forming nanocomposites (NCs). Doping ZnO with silver (Ag) strengthens antibacterial activity because Ag^{+} ions damage

DNA and trigger the production of high levels of ROS, thereby causing oxidative stress in cells. Ag^+ ions also play a role in controlling particle size and structural stability (Cao, 2017; Yan et al., 2018). ZnO–Ag nanocomposites (ZnO–AgNCs) have been reported to exhibit higher antibacterial activity—up to 5% higher than that of pure ZnONPs—and to show potential for medical applications, such as denture coatings to prevent stomatitis (Moraes et al., 2021; Cuadra et al., 2022). Thus, combining ZnO and Ag yields a synergistic antibacterial effect, making ZnO–AgNCs a potential alternative for controlling microbial infections (Pokrowiecki et al., 2022).

The biological synthesis of NPs is emerging as a more environmentally friendly approach, one of which involves the use of plant extracts as bioreducers (Patra & Baek, 2014). Cassava (*Manihot esculenta* Crantz), which is widely cultivated in Indonesia, is known to contain flavonoids such as rutin (Tao et al., 2019). These flavonoids reduce metal ions by donating electrons from their –OH groups and act as capping agents to stabilize the resulting NPs (Edo et al., 2025). Cassava leaf extract has been used to biosynthesize silver nanoparticles (AgNPs) (Wattimena et al., 2022; Oluwatoyin et al., 2025) and magnesium oxide nanoparticles (MgONPs) (Essien et al., 2020). However, its use as a bioreductant for ZnO–AgNCs biosynthesis targeting *P. aeruginosa* has not been extensively explored. In this study, ZnO–AgNCs were biosynthesized using cassava leaf extract, with systematic variation in the concentrations of both the extract and silver nitrate ($AgNO_3$). This study aims to determine the optimal synthesis conditions and evaluate the antibacterial activity of ZnO–AgNCs against *P. aeruginosa*. The results of this study support the development of environmentally friendly antibacterial materials in efforts to control bacterial infections. In the future, this nanomaterial has the potential for widespread application, particularly in the clinical field as an antibacterial agent.

METHODS

This study used cassava leaves (*M. esculenta*) of uniform size from Purwokerto, Central Java; *P. aeruginosa* cultures from the UNS Integrated Laboratory; silver nitrate ($AgNO_3$); zinc acetate dihydrate ($Zn(CH_3CO_2)_2 \cdot 2H_2O$); distilled water; 500 mg ciprofloxacin (Novapharin); Nutrient Agar (Merck); and Mueller-Hinton Agar (Merck). Equipment included a centrifuge (Eppendorf), hotplate, Scanning Electron Microscope with Energy Dispersive X-Ray (SEM-EDX) (Thermo Fisher Scientific, FEI Quanta 250), Particle Size Analyzer (PSA) (Horiba SZ-100), and UV-Vis Spectrophotometer (Hitachi UH5300).

Manihot esculenta leaf extract preparation

Cassava leaf extraction was performed according to the method described by Gonfa & Birhanu (2024), with modifications to the concentration. Cassava leaves were washed with water, cut into small pieces, and oven-dried at 50°C for 48 hours or until completely dry. The dried leaves were then ground and sieved through a 60-mesh sieve to obtain uniformly sized simplicia. The simplicia were mixed with distilled water in a 1:10 ratio, then homogenized on a hot plate at 60°C for 20 minutes. The extract solution was filtered at room temperature. The filtrate was evaporated using a rotary evaporator at 60°C until its volume was reduced to one-quarter of the initial volume. Next, the filtrate was concentrated in a 60°C water bath until the solvent had completely evaporated. A 20% (w/v) stock solution was prepared, then diluted to 5%, 10%, and 15% (v/v) for NCs synthesis. The filtrate was sterilized using a 0.22 µm membrane filter before use in NCs synthesis.

Biosynthesis of ZnO-AgNCs Using *M. esculenta* Leaf Extract

ZnO-AgNCs were synthesized using cassava leaf extract as a bioreductant according to the method described by Makauki et al. (2023), with modifications to the extract concentration. The synthesis was carried out by mixing the precursor solution and the bioreductant. The bioreductant consisted of cassava leaf extract, while the precursors were 0.1 M $AgNO_3$ (1.6987 grams dissolved in distilled water to a final volume of 100 mL) and 0.1 M $Zn(CH_3CO_2)_2 \cdot 2H_2O$ (2.195 grams dissolved in distilled water to 100 mL). Extract solutions at concentrations of 5%, 10%, and 15% were each placed in separate beakers and stirred with a magnetic stirrer. For each concentration, 6 mL of 0.1 M $AgNO_3$ was added, and the mixture was homogenized for 20 minutes. Subsequently, 0.1 M $Zn(CH_3CO_2)_2 \cdot 2H_2O$ was added to reach a final volume of 100 mL, resulting in a final Ag concentration of 6 mM. The pH was adjusted to 7 using 0.1 M NaOH. The beaker was covered with aluminum foil, stirred for 2 hours at 70°C, then cooled to room temperature. The reaction was repeated with a final Ag concentration of 8 mM. The resulting ZnO–AgNCs colloid was purified

by centrifugation at 1600 x g for 15 minutes. The supernatant containing the NCs was used for characterization and antibacterial assay.

Characterization of ZnO-AgNCs

Surface plasmon resonance analysis

Surface Plasmon Resonance (SPR) is detected using a UV–Vis spectrophotometer, which can reveal a characteristic absorption peak and the maximum wavelength (λ max). This is used as an indicator of the nanoparticles' optical behavior of NCs. The purified ZnO–Ag/cassava leaf extract colloids at all concentrations were scanned from 200 to 800 nm to determine their SPR profiles. The observed λ max values represent the wavelengths at which the NCs exhibit maximum absorbance, reflecting the formation and stability of the ZnO–AgNCs. A shift in this peak (redshift or blueshift) may indicate changes in particle size, shape, or interactions with the surrounding matrix, such as the cassava leaf extract.

Particle size analysis (PSA)

The size of ZnO–AgNCs was analyzed using PSA. The ZnO–AgNCs supernatant was purified before testing. A total of 1 mL of the sample solution was transferred into a cuvette and placed in the PSA holder. PSA can display the particle size distribution (average diameter and the polydispersity index (PdI), which measures the uniformity of particle size. A low PdI value (approaching 0), the particles are more homogeneous. Optimal NCs as antibacterial agents are small and homogeneous.

Scanning Electron Microscopy and Energy Dispersive X-ray (SEM-EDX) analysis

SEM was used to analyze particle morphology, while EDX provided both qualitative and quantitative chemical composition data. The sample used was ZnO–AgNCs that had been dried into a powder. SEM produces a micrograph of the surface morphology of ZnO–AgNCs at various magnifications, which are used to assess particle distribution and homogeneity. ZnO–AgNCs are defined as particles ranging in size from 1 to 100 nm, exhibiting circular, star-shaped, rod-shaped, or other morphologies. EDX spectroscopy can confirm the relative proportions of Zn, O, and Ag in the NCs structure.

Antibacterial activity assay

The antibacterial activity was evaluated using the disc diffusion method on Mueller-Hinton Agar (MHA). *P. aeruginosa* cultures were refreshed by subculturing on nutrient agar and incubating at 37°C for 24 hours. A single loopful of bacterial culture was suspended in 0.8% physiological saline and adjusted to a turbidity equivalent to 0.5 McFarland standard (1.5×10^8 CFU/mL). Bacteria were inoculated onto MHA by streaking with a sterile swab dipped in the bacterial suspension. Sterile disc papers (6 mm diameter) were loaded with 10 µl of each test solution: ZnONPs supernatant, ZnO-AgNCs supernatant, ciprofloxacin (positive control), cassava leaf extract, and distilled water (negative control). The discs were then placed on the surface of the inoculated media. Antibacterial activity was indicated by a clear inhibition zone surrounding the discs. The diameter of the inhibition zone was measured after 24 hours of incubation at 37°C.

RESULTS AND DISCUSSION

Characteristics of ZnO-AgNCs biosynthesized from cassava leaf extract

Visual observations served as preliminary evidence for the formation of zinc oxide – silver nanocomposites (ZnO–AgNCs). The ZnO–AgNCs were synthesized by reacting cassava leaf extract at concentrations of 5%, 10%, and 15% with $AgNO_3$ precursors (6 mM and 8 mM) and Zn(CH3COO)2·2H2O at 80°C for 2 hours. A colour change in the solution during the reaction indicated the reduction of metal ions and the formation of nanoscale particles suspended in the medium.

The ZnO–AgNCs colloid appears increasingly opaque as the concentrations of the extract and $AgNO_3$ increase (Figure 1). Cassava leaf extract contains various phytochemical compounds, including flavonoids and phenols. These phytochemicals act as bioreducers capable of reducing metal ions through electron transfer from functional groups such as hydroxyl (-OH), thereby converting Ag^+ and Zn^{2+} to Ag^0 and ZnO. The increasingly intense color of the colloid serves as a qualitative indication that the synthesis of ZnO–AgNCs was successful, and this change forms the initial basis for further characterization.

The identification of ZnO–AgNCs relies on the specific characteristics of the particles' Surface Plasmon Resonance (SPR). This phenomenon generates a distinctive peak in the UV-Vis spectrum, and the maximum wavelength (λ max) serves as an indicator of the nanoparticles' optical properties. Measurements were conducted within the 200-800 nm range. The λ max values are

presented in Table 1, the corresponding spectral changes are illustrated in Figure 2.

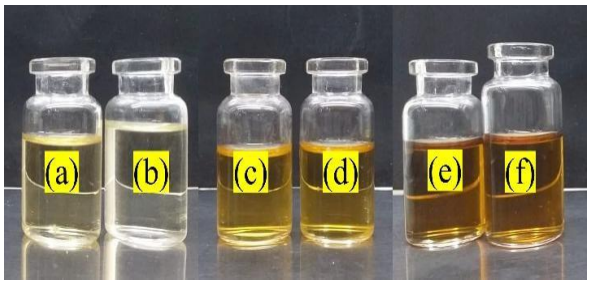

Figure 1. ZnO–AgNCs colloids synthesized using varying concentrations of cassava leaf extract and $AgNO_3$: (a) 5% extract with 6 mM $AgNO_3$, (b) 5% extract with 8 mM $AgNO_3$, (c) 10% extract with 6 mM $AgNO_3$, (d) 10% extract with 8 mM $AgNO_3$, (e) 15% extract with 6 mM $AgNO_3$, and (f) 15% extract with 8 mM $AgNO_3$.

The maximum wavelength of NCs from all treatment variations formed was in the range of 331–405 nm (Table 3). This value indicates the presence of the SPR phenomenon of ZnO–AgNCs. This range corresponds to the typical ZnO peak at 330–390 nm (Król et al., 2017) and is close to the characteristic wavelength of AgNPs, typically 400–450 nm (Eid et al., 2020). This indicates successful NC formation, although the peak position may shift due to interactions between ZnO and Ag within the material.

Table 1. Peak wavelength of ZnO–AgNCs

Treatments	λ max (nm)
5% extract + 6 mM $AgNO_3$	331.33 ± 8.08
5% extract + 8 mM $AgNO_3$	331.66 ± 6.02
10% extract + 6 mM $AgNO_3$	370.00 ± 6.24
10% extract + 8 mM $AgNO_3$	370.00 ± 8.18
15% extract + 6 mM $AgNO_3$	405.66 ± 6.24
15% extract + 8 mM $AgNO_3$	399.00 ± 4.61

Note: Values represent the mean ± standard deviation calculated from three replicates.

Figure 2 demonstrates that increasing both extract and $AgNO_3$ concentrations shifts λmax to longer wavelengths and enhances absorbance intensity. Treatments with 5% extract combined with 6 mM or 8 mM $AgNO_3$ exhibited lower λmax values and absorbance compared to those with higher concentrations. A shift in λmax towards longer wavelengths indicates an increase in particle size or the occurrence of agglomeration, whereas a shift toward shorter wavelengths indicates smaller particle size. The increase in absorbance intensity may be due to an increase in the number of particles formed, which is associated with a higher availability of reducing agents. According to Saha et al. (2021) increase in SPR band intensity is associated with high extract concentration, which causes the peak to shift toward longer wavelengths. The increase in SPR intensity also indicates that the formation and growth of NCs occur more rapidly. On the other hand, the addition of $AgNO_3$ also affects the optical properties of NCs. The presence of Ag can increase the electron density on the ZnO surface, which ultimately causes a shift in the λmax value Gonfa & Birhanu, 2024). Particle size and the polydispersity index (PdI) were then further confirmed using a particle size analyzer (PSA).

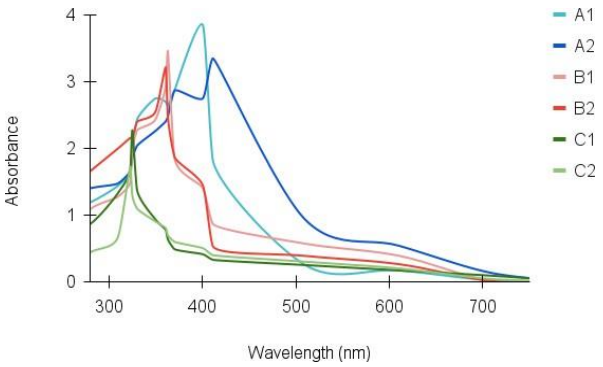

Figure 2. Wavelengths of ZnO–AgNCs synthesized with different extract concentrations and $AgNO_3$ levels: (A1) 5% extract, 6 mM $AgNO_3$; (A2) 5% extract, 8 mM $AgNO_3$; (B1) 10% extract, 6 mM $AgNO_3$; (B2) 10% extract, 8 mM $AgNO_3$; (C1) 15% extract, 6 mM $AgNO_3$; (C2) 15% extract, 8 mM $AgNO_3$.

Table 2 presents the NPs size distributions for each biosynthesis condition. Particle sizes ranged from 30.05–85.25 nm, indicating that all treatments yielded NPs (<100 nm). The 10% extract + 6 mM $AgNO_3$ combination had the smallest particle size (30.05 nm), while the 15% extract + 8 mM $AgNO_3$ combination had the largest particle size (85.25 nm). This indicates that the concentrations of the bioreductant and precursor play a significant role in determining particle growth and final size.

Table 2. Dominant particle size and polydispersity index for ZnO–AgNCs

Treatments	Dominant particle (d.nm)	Polydispersity index
5% extract + 6 mM $AgNO_3$	50.91	0.64
5% extract + 8 mM $AgNO_3$	48.04	0.67
10% extract + 6 mM $AgNO_3$	30.05	0.65
10% extract + 8 mM $AgNO_3$	53.23	0.48
15% extract + 6 mM $AgNO_3$	62.07	0.8
15% extract + 8 mM $AgNO_3$	85.25	1.0

The PdI values indicate that treatments with 5% and 10% extract concentrations have a PdI <0.7, which is characteristic of a homogeneous size distribution (monodispersity). In contrast, the 15% extract concentration had a PdI >0.7, indicating a broader size distribution (polydispersity) and a higher likelihood of agglomeration (Nidhin et al., 2008). In addition, 15% extract concentration showed a graph with a tail distribution above 100 nm, which is consistent with a high PdI value (Figure 3). Nevertheless, the majority of the size distribution remained below 100 nm, indicating that most of the particles formed still fall within the NPs range. Furthermore, in all treatments, the dominant size was also below 100 nm, so it can be concluded that the resulting particles are generally of nanoscale size.

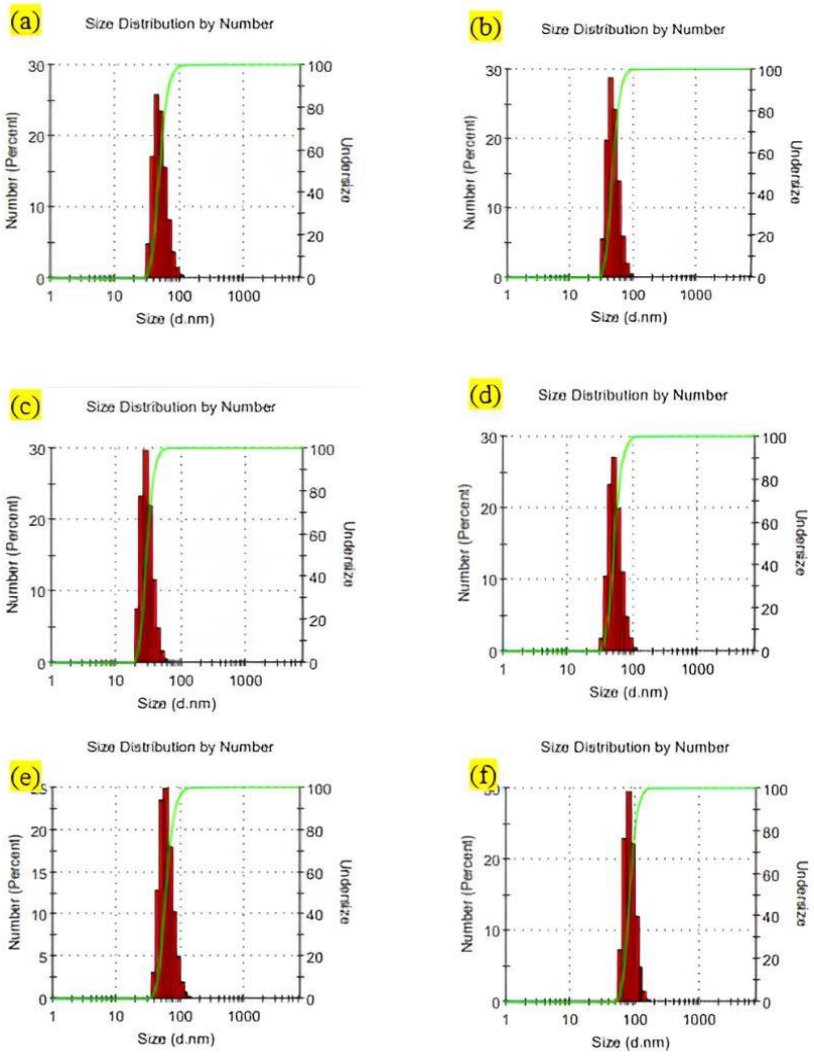

Figure 3. Size distribution curves of ZnO–AgNCs synthesized using varying concentrations: (a) 5% extract with 6 mM $AgNO_3$, (b) 5% extract with 8 mM $AgNO_3$, (c) 10% extract with 6 mM $AgNO_3$, (d) 10% extract with 8 mM $AgNO_3$, (e) 15% extract with 6 mM $AgNO_3$, and (f) 15% extract with 8 mM $AgNO_3$.

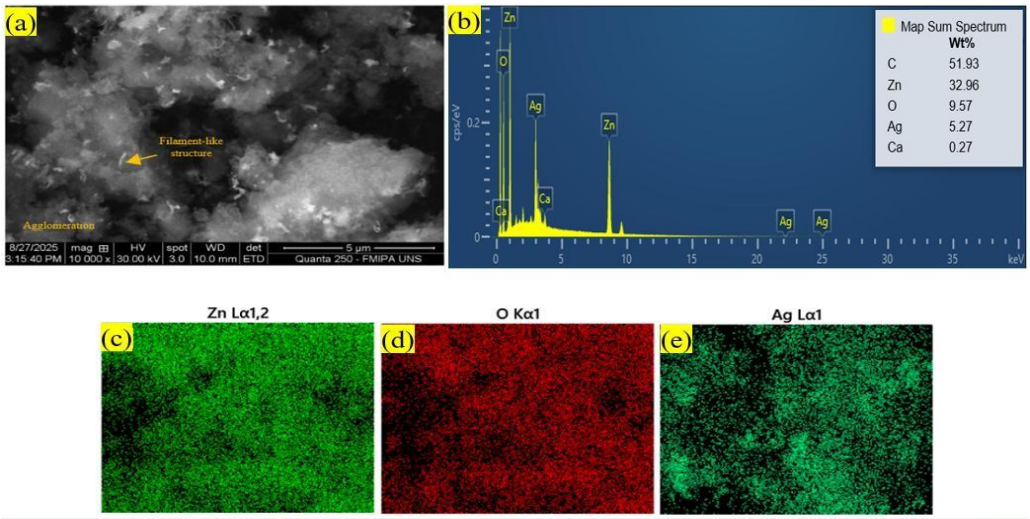

Figure 4. (a) SEM image of ZnO–AgNCs showing irregular and agglomerated morphology, (b) EDX spectrum confirming the presence of elements, (c) Zn elemental mapping, (d) O elemental mapping, (e) Ag elemental mapping.

The surface structure and elemental composition of the ZnO–AgNCs were then analyzed using scanning electron microscopy–energy dispersive X-ray spectroscopy (SEM–EDX). A non-homogeneous structure was observed with irregularly shaped particles dominating the surface of the ZnO–AgNCs (Figure 4a). The difficulty in observing interparticle gaps indicates that the particles have agglomerated. Additionally, filament-like structures with bright contrast were observed, indicating topographical differences in particle topography and uneven particle growth, resulting in heterogeneous morphology (Kowoll et al., 2017). Agglomeration occurs due to interparticle attractive forces, particularly in unstable NPs, influenced by van der Waals interactions and the formation of chemical bonds (Zare, 2016).

The EDX spectrum reveals constituent elements in the particles, including 32.96% Zn, 9.57% O, and 5.27% Ag (Figure 4b). The presence of Zn and O confirms the formation of ZnO, while the presence of Ag indicates the successful incorporation of Ag into the ZnO matrix. The lower percentage of Ag compared to Zn is consistent with the initial synthesis composition, ZnO as the main component and Ag as the dopant. EDX also detected 51.93% C and 0.27% Ca, which likely originated from residual organic compounds in the cassava leaf extract used as a bioreductant. This indicates that nature-based synthesis processes often leave organic residues even after purification. However, the Zn and Ag in the spectrum still indicate the successful bonding of these two metals on the particle surface.

The distribution of the elements is shown in the elemental mapping results, including mapping of Zn (Figure 4c), O (Figure 4d), and Ag (Figure 4e). The distribution of these elements is relatively uniform across the entire observed area. The overlapping distribution patterns of Zn and O indicate a correlation between the two within the ZnO structure. The uniform distribution of Ag on the material's surface indicates that the Ag doping was successful and that the atoms are well dispersed within the ZnO matrix.

Antibacterial activities against *P. aeruginosa*

The ability of ZnO–AgNCs to inhibit the growth of *P. aeruginosa* was evident from the presence of a clear zone (inhibition zone) around the disc (Figure 7). A wide inhibition zone indicates high antibacterial activity. The results shown in Table 3 indicate that all ZnO–AgNCs treatments produced wider inhibition zones than distilled water (0 mm) and 15% cassava leaf extract (5.03 ± 0.16 mm), indicating that the antibacterial activity originates from the NCs. Ciprofloxacin produced the largest inhibition zone (43.98 ± 1.68 mm), confirming its effectiveness as a commercial antibiotic against *P. aeruginosa*. Meanwhile, the ZnONPs produced an inhibition zone of 12.48 ± 1.23 mm, which was greater than that of the 15% extract but smaller than that of nearly all ZnO–AgNCs treatments.

The antibacterial activity of ZnO–AgNCs is significantly greater than that of ZnONPs. This is due to a synergistic effect involving the simultaneous release of Ag^{+} and Zn^{2+} ions. These ions diffuse and interact with the cell walls and

membranes of bacteria, disrupting the ionic balance and enzymatic functions within the cells (Busila et al., 2023). Ag also plays a role in reducing crystal size while increasing the material's active surface area, which can enhance its antibacterial effectiveness (Cuadra et al., 2022).

Table 3. Inhibition zone diameter of ZnO–AgNCs against *P. aeruginosa*

Treatment	Inhibition zone (mm)
5% extract + 6 mM $AgNO_3$	15.16 ± 0.85^{ef}
5% extract + 8 mM $AgNO_3$	15.83 ± 0.64^{f}
10% extract + 6 mM $AgNO_3$	14.10 ± 0.75^{def}
10% extract + 8 mM $AgNO_3$	13.05 ± 0.58^{cde}
15% extract + 6 mM $AgNO_3$	12.50 ± 0.60^{cd}
15% extract + 8 mM $AgNO_3$	11.55 ± 0.54^{c}
Aquades	
Ciprofloxacin	43.98 ± 1.68^{g}
ZnONPs	12.48 ± 1.23^{cd}
15% extract	5.03 ± 0.16^{b}

Note: Values are the average ± standard deviation from three replicates. Numbers followed by different letters indicate significant differences at the 95% significance level.

Measurements of the ZnO–AgNCs inhibition zone showed that the combination of 5% extract + 8 mM $AgNO_3$ yielded the largest inhibition zone (15.83 ± 0.64 mm). This value was significantly greater than most other combinations and represents the optimal condition. In contrast, ZnO–AgNCs prepared with higher extract concentrations exhibited reduced inhibition zones. This diminished antibacterial activity is attributed to elevated levels of reducing compounds, which promote particle agglomeration and, consequently, reduce the nanocomposites' active surface area. This interpretation is corroborated by PSA data, which show larger particles and a greater propensity for agglomeration at elevated extract concentrations. All ZnO–AgNCs combination treatments were classified as strong (10–25 mm) (Davis & Stout, 1971).

In addition to the formation of an inhibition zone, certain treatments induced a color change in the medium from clear to blue-green after the incubation period (Figure 7). This phenomenon is attributed to the production of pyocyanin by *P. aeruginosa*. Pyocyanin, a blue-green phenazine pigment synthesized by 90–95% of *P. aeruginosa* strains, functions as a bacterial virulence factor and facilitates quorum sensing (Mudaliar & Bharath Prasad, 2024). Moreover, this pigment contributes to the bacterial cell's defense response against nanoparticle (NP) exposure. Pyocyanin interacts with metal ions released from NPs, thereby partially neutralizing their antibacterial activity (Busila et al., 2023).

The medium remained clear during ZnO–AgNCs treatment at a 5% extract concentration, resulting in smaller particles and a larger inhibition zone. In contrast, a more pronounced blue-green color was observed in the ZnO–AgNCs treatment medium at 10% and 15% extract concentrations, which produced larger particle sizes and smaller inhibition zones. This demonstrates that the particle size of ZnO–AgNCs significantly affects their antibacterial efficacy. Smaller particle sizes increase the specific surface area, thereby providing more active sites for direct interaction with bacterial cell membranes. Therefore, optimizing the synthesis conditions of NCs is crucial for enhancing antibacterial activity and as an antivirulence intervention strategy against *P. aeruginosa* by inhibiting pyocyanin production.

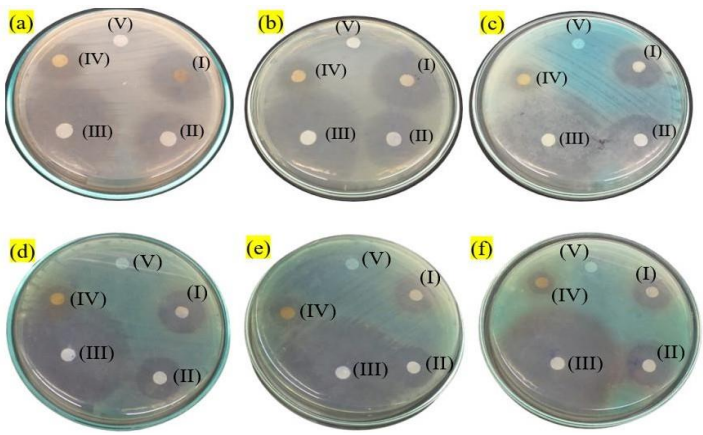

Figure 7. Inhibition zone of (I) ZnO–AgNCs ((a) 5% extract + 6 mM $AgNO_3$, (b) 5% extract + 8 mM $AgNO_3$, (c) 10% extract + 6 mM $AgNO_3$, (d) 10% extract + 8 mM $AgNO_3$, (e) 15% extract + 6 mM $AgNO_3$, (f) 15% extract + 8 mM $AgNO_3$), (II) ZnONPs, (III) ciprofloxacin, (IV) 15% extract, (V) aquades.

This study complements previous research by demonstrating that ZnO–AgNCs synthesized using cassava leaf extract exhibit antibacterial activity against *P. aeruginosa*. Their effectiveness is influenced by factors such as the concentrations of bioreductant and precursor. This research supports the potential to develop nanomaterial-based antibacterial agents and to use plant extracts as environmentally friendly bioreductants. The ability of NCs to inhibit bacterial growth also has potential applications in infection control and public health. Therefore, this research supports the Sustainable Development Goal (SDG) on Good Health and Well-being (No. 3) by developing effective antibacterial agents.

CONCLUSION

The results of the study indicate that variations in the concentrations of the extract and $AgNO_3$ affect the physicochemical properties and antibacterial effects. ZnO-AgNCs were able to inhibit the growth of *P. aeruginosa*, as evidenced by the presence of inhibition zones larger than 10 mm. However, further studies are needed to investigate the antibacterial mechanism, evaluate toxicity and biocompatibility, and explore potential biomedical applications. In addition, more comprehensive physicochemical characterization, including X-ray diffraction (XRD), Fourier-transform infrared spectroscopy (FTIR), and zeta potential analysis, is recommended to further verify the crystal structure, identify surface functional groups involved in nanoparticle formation, and evaluate the colloidal stability of the synthesized ZnO–Ag nanocomposites. Such analyses would provide a more complete understanding of their physicochemical properties and support their future development for biomedical applications.

ACKNOWLEDGEMENT

This research was partially funded by Sebelas Maret University through the Group Research Grant (PKGR-UNS), non-APBN funds, 2026, under the contract number 462/UN27.22/PT.01.03/2026.

AUTHOR CONTRIBUTION STATEMENT

All authors contributed significantly to the work reported in this manuscript. WRH, AS, and AP designed the experiments. WRH performed the research. WRH, AS, and AP analyzed the data. WRH, AS, and AP wrote the manuscript. MA reviewed, proofread, and revised the manuscript. All authors read and approved the final version of the manuscript and agreed to be accountable for all aspects of the work.

CONFLICT OF INTEREST STATEMENT

The authors declare that there is no conflict of interest regarding the publication of this paper.

USE OF ARTIFICIAL INTELLIGENCE (AI)-ASSISTED TECHNOLOGY

The authors declare that no artificial intelligence (AI) tools were used in the generation, analysis, or writing of this manuscript. All aspects of the research, including data collection, interpretation, and manuscript preparation, were carried out entirely by the authors without the assistance of AI-based technologies.

REFERENCES

Busila, M., Musat, V., Alexandru, P., Romanitan, C., Brincoveanu, O., Tucureanu, V., Mihalache, I., Iancu, A. V., & Dediu, V. (2023). antibacterial and photocatalytic activity of ZnO/Au and ZnO/Ag nanocomposites. *International Journal of Molecular Sciences*, *24*(23), 1–15. https://doi.org/10.3390/ijms242316939

Cao, Huiliang. (2017). *Silver nanoparticles for antibacterial devices : biocomparibility and toxicity*. CRC Press.

Chausali, N., Saxena, J., & Prasad, R. (2022). Recent trends in nanotechnology applications of bio-based packaging. *Journal of Agriculture and Food Research*, *7*, 1–14. https://doi.org/10.1016/j.jafr.2021.100257

Cuadra, J. G., Scalschi, L., Vicedo, B., Guc, M., Izquierdo-Roca, V., Porcar, S., Fraga, D., & Carda, J. B. (2022). ZnO/Ag nanocomposites with enhanced antimicrobial activity. *Applied Sciences*, *12*(10), 1–15. https://doi.org/10.3390/app12105023

Davis, W. W., & Stout, T. R. (1971). Disc plate method of microbiological antibiotic assay ii. novel procedure offering improved accuracy'. *Applied Microbiology*, *22*(4), 659–665. https://doi.org/10.1128/am.22.4.659-665.1971.

Edo, G. I., Mafe, A. N., Ali, A. B. M., Akpoghelie, P. O., Yousif, E., Isoje, E. F., Igbuku, U.
A., Ismael, S. A., Essaghah, A. E. A., Ahmed, D. S., Ozsahin, D. U., Umar, H., & Alamiery, A. A. (2025). Green biosynthesis of nanoparticles

using plant extracts: mechanisms, advances, challenges, and applications. *BioNanoScience*, *15*(2), 267–304. https://doi.org/10.1007/s12668-025-01883-w

Eid, A. M., Fouda, A., Niedbała, G., Hassan, S. E. D., Salem, S. S., Abdo, A. M., Hetta, H. F., & Shaheen, T. I. (2020). Endophytic *Streptomyces laurentii* mediated green synthesis of Ag-NPs with antibacterial and anticancer properties for developing functional textile fabric properties. *Antibiotics*, *9*(10), 1–18. https://doi.org/10.3390/antibiotics9100641

Essien, E. R., Atasie, V. N., Okeafor, A. O., & Nwude, D. O. (2020). Biogenic synthesis of magnesium oxide nanoparticles using *Manihot esculenta* (Crantz) leaf extract. *International Nano Letters*, *10*(1), 43–48. https://doi.org/10.1007/s40089-019-00290-w

Gonfa, M. H., & Birhanu, A. L. (2024). Green synthesis, characterization and antibacterial evaluation of ZnO and Ag-doped ZnO nanoparticles using *Ruta chalepensis* leaf extract. *Green Chemistry Letters and Reviews*, *17*(1),1–14. https://doi.org/10.1080/17518253.2024.2412613

Khan, I., Saeed, K., & Khan, I. (2019). Nanoparticles: Properties, applications and toxicities. *Arabian Journal of Chemistry*, *12*(7), 908–931. https://doi.org/10.1016/j.arabjc.2017.05.011

Kowoll, T., Müller, E., Fritsch-Decker, S., Hettler, S., Störmer, H., Weiss, C., & Gerthsen, D. (2017). Contrast of backscattered electron SEM images of nanoparticles on substrates with complex structure. *Scanning*, *2017*(1), 1–12. https://doi.org/10.1155/2017/4907457

Król, A., Pomastowski, P., Rafińska, K., Railean-Plugaru, V., & Buszewski, B. (2017). Zinc oxide nanoparticles: Synthesis, antiseptic activity and toxicity mechanism. In *Advances in Colloid and Interface Science*, *249*(1), 37–52. https://doi.org/10.1016/j.cis.2017.07.033

Makauki, E., Mtavangu, S. G., Basu, O. D., Rwiza, M., & Machunda, R. (2023). Facile biosynthesis of Ag–ZnO nanocomposites using *Launaea cornuta* leaf extract and their antimicrobial activity. *Discover Nano*, *18*(1), 142–157. https://doi.org/10.1186/s11671-023-03925-2

Moraes, G., Zambom, C., & Siqueira, W. L. (2021). Nanoparticles in dentistry: A comprehensive review. *Pharmaceuticals*, *14*(8), 1–29. https://doi.org/10.3390/ph1408075 2

Moser, C., Jensen, P. Ø., Thomsen, K., Kolpen, M., Rybtke, M., Lauland, A. S., Trøstrup, H., & Tolker-Nielsen, T. (2021). Immune responses to *Pseudomonas aeruginosa* biofilm infections. *Immunology*, *12*(625597), 1–15. https://doi.org/10.3389/fimmu.2021.625597

Mudaliar, S. B., & Bharath Prasad, A. S. (2024). A biomedical perspective of pyocyanin from *Pseudomonas aeruginosa*: its applications and challenges. *Journal of Microbiology and Biotechnology*, *40*(3), 1–23. https://doi.org/10.1007/s11274-024-03889-0

Nidhin, M., Indumathy, R., Sreeram, K. J., & Nair, B. U. (2008). Synthesis of iron oxide nanoparticles of narrow size distribution on polysaccharide templates. *Bull. Mater. Sci*, *31*(1), 93–96. https://doi.org/10.1007/s12034-008-0016-2

Oluwatoyin, A. C., Dada, A. O., Eneojo, T. B., Oluseyi, A. K., & Oluwaseyi, O. (2025). Green synthesis of silver nanoparticles using sustainable *Manihot esculenta* leaf extract: phytochemical screening and effect of operational parameters. *NIPES - Journal of Science and Technology Research*, *7*(1), 2555–2561. https://doi.org/10.37933/nipes/7.4.2025.SI302

Palanisamy, N. K., Ferina, N., Amirulhusni, A. N., Mohd-Zain, Z., Hussaini, J., Jian Ping, L., & Durairaj, R. (2014). Antibiofilm properties of chemically synthesized silver nanoparticles found against *Pseudomonas aeruginosa*. *Journal of Nanobiotechnology*, *12*(2), 1–7. http://www.jnanobiotechnology.com/content/12/1/2

Patra, J. K., & Baek, K. H. (2014). Green nanobiotechnology: factors affecting synthesis and characterization techniques. *Journal of Nanomaterials*, *2014*(1), 417305–417316. https://doi.org/10.1155/2014/417305

Pokrowiecki, R., Szałaj, U., Fudala, D., Zaręba, T., Wojnarowicz, J., Łojkowski, W., Tyski, S., Dowgierd, K., & Mielczarek, A. (2022). Dental implant healing screws as temporary oral drug delivery systems for decrease of infections in the area of the head and neck. *International Journal of Nanomedicine*, *17*(1), 1679–1693. https://doi.org/10.2147/IJN.S333720

Qin, S., Xiao, W., Zhou, C., Pu, Q., Deng, X., Lan, L., Liang, H., Song, X., & Wu, M. (2022). *Pseudomonas aeruginosa*: pathogenesis, virulence factors, antibiotic resistance, interaction with host, technology advances and emerging therapeutics. *Signal Transduction and Targeted Therapy*, *7*(1), 1–27. https://doi.org/10.1038/s41392-022-01056-1

Reynolds, D., & Kollef, M. (2021). The epidemiology and pathogenesis and treatment of *Pseudomonas aeruginosa* infections: an update. In *Drugs*, *81*(18), 2117–2131. https://doi.org/10.1007/s40265-021-01635-6

Saha, P., Mahiuddin, M., Islam, A. B. M. N., & Ochiai, B. (2021). Biogenic synthesis and catalytic efficacy of silver nanoparticles based on peel extracts of *Citrus macroptera* fruit. *ACS Omega*, *6*(28), 18260–18268. https://doi.org/10.1021/acsomega.1c02149

Moraes, G., Zambom, C., & Siqueira, W. L. (2021). Nanoparticles in dentistry: A

comprehensive review.*Pharmaceuticals*,*14*(8),1–29. https://doi.org/10.3390/ph1408075 2

Moser, C., Jensen, P. Ø., Thomsen, K., Kolpen, M., Rybtke, M., Lauland, A. S., Trøstrup, H., & Tolker-Nielsen, T. (2021). Immune responses to *Pseudomonas aeruginosa* biofilm infections. *Immunology*, *12*(625597), 1–15. https://doi.org/10.3389/fimmu.2021.625597

Mudaliar, S. B., & Bharath Prasad, A. S. (2024). A biomedical perspective of pyocyanin from *Pseudomonas aeruginosa*: its applications and challenges. *Journal of Microbiology and Biotechnology*, *40*(3), 1–23. https://doi.org/10.1007/s11274-024-03889-0

Nidhin, M., Indumathy, R., Sreeram, K. J., & Nair, B. U. (2008). Synthesis of iron oxide nanoparticles of narrow size distribution on polysaccharide templates. *Bull. Mater. Sci*, *31*(1), 93–96. https://doi.org/10.1007/s12034-008-0016-2

Oluwatoyin, A. C., Dada, A. O., Eneojo, T. B., Oluseyi, A. K., & Oluwaseyi, O. (2025). Green synthesis of silver nanoparticles using sustainable *Manihot esculenta* leaf extract: phytochemical screening and effect of operational parameters. *NIPES - Journal of Science and Technology Research*, *7*(1), 2555–2561. https://doi.org/10.37933/nipes/7.4.2025.SI302

Palanisamy, N. K., Ferina, N., Amirulhusni, A. N., Mohd-Zain, Z., Hussaini, J., Jian Ping, L., & Durairaj, R. (2014). Antibiofilm properties of chemically synthesized silver nanoparticles found against *Pseudomonas aeruginosa*. *Journal of Nanobiotechnology*, *12*(2), 1–7. http://www.jnanobiotechnology.com/content/12/1/2

Patra, J. K., & Baek, K. H. (2014). Green nanobiotechnology: factors affecting synthesis and characterization techniques. *Journal of Nanomaterials*, *2014*(1), 417305–417316. https://doi.org/10.1155/2014/417305

Pokrowiecki, R., Szałaj, U., Fudala, D., Zaręba, T., Wojnarowicz, J., Łojkowski, W., Tyski, S., Dowgierd, K., & Mielczarek, A. (2022). Dental implant healing screws as temporary oral drug delivery systems for decrease of infections in the area of the head and neck. *International Journal of Nanomedicine*, *17*(1), 1679–1693. https://doi.org/10.2147/IJN.S333720

Qin, S., Xiao, W., Zhou, C., Pu, Q., Deng, X., Lan, L., Liang, H., Song, X., & Wu, M. (2022). *Pseudomonas aeruginosa*: pathogenesis, virulence factors, antibiotic resistance, interaction with host, technology advances and emerging therapeutics. *Signal Transduction and Targeted Therapy*, *7*(1), 1–27. https://doi.org/10.1038/s41392-022-01056-1

Reynolds, D., & Kollef, M. (2021). The epidemiology and pathogenesis and treatment of *Pseudomonas aeruginosa* infections: an update. In *Drugs*, *81*(18), 2117–2131. https://doi.org/10.1007/s40265-021-01635-6

Saha, P., Mahiuddin, M., Islam, A. B. M. N., & Ochiai, B. (2021). Biogenic synthesis and catalytic efficacy of silver nanoparticles based on peel extracts of *Citrus macroptera* fruit. *ACS Omega*, *6*(28), 18260–18268. https://doi.org/10.1021/acsomega.1c02149

Sali, R. K., Pujar, M. S., Patil, S., & Sidarai, A. H. (2021). green synthesis of zno and ag-zno nanoparticles using *Macrotyloma uniflorum:* evaluation of antibacterial activity. *Advanced Materials Letters*, *12*(7), 1–7. https://doi.org/10.5185/amlett.2021.071645

Sirelkhatim, A., Mahmud, S., Seeni, A., Kaus, N. H. M., Ann, L. C., Bakhori, S. K. M., Hasan, H., & Mohamad, D. (2015). Review on zinc oxide nanoparticles: Antibacterial activity and toxicity mechanism. *Nano-Micro Letters*, *7*(3), 219–242. https://doi.org/10.1007/s40820-015-0040-x

Tao, H., Cui, B., Zhang, H., Bekhit, A. E. D., & Lu, F. (2019). Identification and characterization of flavonoids compounds in cassava leaves (*Manihot esculenta* Crantz) by HPLC/FTICR-MS. *International Journal of Food Properties*, *22*(1), 1134–1145. https://doi.org/10.1080/10942912.2019.1626879

Thi, M. T. T., Wibowo, D., & Rehm, B. H. A. (2020). *Pseudomonas aeruginosa* biofilms. *International Journal of Molecular Sciences*, *21*(22), 1–25. https://doi.org/10.3390/ijms21228671

Wattimena, S. C., Ayuningrum, D. A., Latuasan, L. Y., Samson, E., & Patty, P. J. (2022). Properties of bio-silver nanoparticles mediated by tuber

and leaf extracts of *Manihot esculenta. Biosaintifika,* 14(2), 271-278. https://doi.org/10.15294/biosaintifika. v14i2.37667

Yan, X., He, B., Liu, L., Qu, G., Shi, J., Hu, L., & Jiang, G. (2018). Antibacterial mechanism of silver nanoparticles in: *Pseudomonas aeruginosa*: Proteomics approach. *Metallomics*, *10*(4), 557–564. https://doi.org/10.1039/c7mt00328e

Zare, Y. (2016). Study of nanoparticles aggregation/agglomeration in polymer particulate nanocomposites by mechanical properties. *Composites Part A: Applied Science and Manufacturing*, *84*(1), 158–164. https://doi.org/10.1016/j.compositesa.2016.01.020